58 *Biochemistry* **2010,** *49,* 58–67
DOI: 10.1021/bi901872s

BIOCHEMISTRY
including biophysical chemistry & molecular biology
Article

Production and Characterization of a Functional Putidaredoxin Reductase−Putidaredoxin Covalent Complex†

Inna Y. Churbanova,‡,∥ Thomas L. Poulos,‡,§ and Irina F. Sevrioukova*,‡

‡*Department of Molecular Biology and* §*Departments of Chemistry and Pharmaceutical Sciences, University of California, Irvine, California 92697-3900.* ∥*Present address: PRA International, Moscow 125445, Russia.*

Received October 31, 2009; Revised Manuscript Received December 1, 2009

ABSTRACT: In the cytochrome P450cam-dependent monooxygenase system from *Pseudomonas putida*, putidaredoxin (Pdx) shuttles electrons between putidaredoxin reductase (Pdr) and P450cam and, thus, must form transient complexes with both partners. 1-Ethyl 3-[3-(dimethylamino)propyl]carbodiimide (EDC) was found to promote formation of stoichiometric Pdr−Pdx complexes only when carboxyl groups on Pdx were activated. The yield of the EDC-mediated cross-link depended on the Pdx variant used and the redox state of both partners, decreasing in the following order: Pdr^{ox}−Pdx^{ox} > Pdr^{ox}−Pdx^{red} ≥ Pdr^{red}−Pdx^{red}. The Pdr−Pdx C73S/C85S conjugate was purified and characterized. Compared to the equimolar mixture of intact Pdr and Pdx, the fusion protein was more efficient in electron transfer to cytochrome *c* and, in the presence of saturating levels of P450cam, more effectively supported camphor hydroxylation. On the basis of our results, we conclude that (i) the cross-linked complex is physiologically relevant and represents a suitable model for mechanistic studies, (ii) molecular recognition between Pdr and Pdx is redox-controlled and assisted by the $Glu72^{Pdx}$−$Lys409^{Pdr}$ charge−charge interactions, and (iii) the high specificity of the Pdr−Pdx couple may be due to finely tuned interactions at the protein−protein interface resulting in only one strongly preferred docking orientation leading to efficient FAD-to-[2Fe-2S] electron transfer.

Putidaredoxin reductase (Pdr,[1] 45 kDa) belongs to a class of bacterial oxygenase-coupled NADH-dependent ferredoxin reductases that adopt the same fold as the glutathione reductase family of enzymes (*1*). In *Pseudomonas putida*, Pdr transfers electrons from NADH to a [2Fe-2S] ferredoxin, putidaredoxin (Pdx, 11 kDa), which in turn reduces a terminal oxygenase, cytochrome P450cam, catalyzing regio- and stereospecific hydroxylation of camphor by consuming two electrons and molecular oxygen per reaction cycle (*2*). To provide tight coupling and efficient turnover of P450cam monooxygenase [2000 min^{-1} (*3*)], Pdx must form productive electron transfer (ET) complexes with both partners. The functioning of the Pdx−P450cam couple has been extensively studied and is well-understood. The detailed mechanism of the Pdr−Pdx pair, however, remains to be established. Mechanistic studies of Pdr and Pdx are important for improving our understanding of how P450cam and other oxygenase- and P450-dependent ET systems catalyze oxidation of a wide range of organic compounds, frequently used for biotechnological applications and bioremediation (*4*−*11*). Investigation of the Pdr−Pdx interaction could also help to clarify how the optimal balance between high specificity and high effectiveness of interprotein ET is achieved.

Pdr-to-Pdx ET is highly efficient [16000 min^{-1} (*12*)], and both partners have low cross reactivity with other flavoproteins and iron−sulfur proteins (*13*−*16*). Utilization of kinetic, chemical modification, mutagenesis, NMR, isothermal calorimetry, laser-flash photolysis, optical biosensor, and computer modeling techniques for studying the Pdr−Pdx mechanism led to a general conclusion that formation of a complex between the partners is driven by both ionic and nonionic interactions (*17*−*27*). After determining the X-ray structures of Pdr and Pdx (*28*−*30*), we developed a computer model for the ET complex and tested its validity by kinetic and protein engineering techniques (*27*). The modeling study suggested that steric complementarity plays an important role in the Pdr−Pdx association and that Tyr33, Arg66, and Trp106 are key surface residues in Pdx that prevent its tight binding and facilitate dissociation upon reduction.

Despite these advances, the precise binding mode, docking sites, and interacting residues in Pdr and Pdx remain unknown. To gain deeper insight into the mechanism of molecular recognition and interprotein ET in the Pdr−Pdx pair, we undertook a cross-linking study to trap a physiologically relevant Pdr−Pdx covalent complex for detailed structure−function studies. The results of this effort are the topic of this paper.

EXPERIMENTAL PROCEDURES

Protein Preparation. Protein expression and purification were conducted as described previously (*12*, *27*, *28*). K409A and

†This study was supported by the National Institutes of Health Grants GM67637 (I.F.S.) and GM33688 (T.L.P.).

*To whom correspondence should be addressed: Department of Molecular Biology and Biochemistry, 3205 McGaugh Hall, University of California, Irvine, CA 92697-3900. Telephone: (949) 824-1953. Fax: (949) 824-3280. E-mail: sevrioui@uci.edu.

[1]Abbreviations: Pdr, Pdr^{ox}, Pdr^{sq}, and Pdr^{red}, putidaredoxin reductase and its oxidized, one-electron-reduced, and two-electron-reduced forms, respectively; Pdx, Pdx^{ox}, and Pdx^{red}, putidaredoxin and its oxidized and reduced forms, respectively; P450cam, camphor hydroxylating cytochrome P450 from *Pseudomonas putida*; ET, electron transfer; MBS, *m*-maleimidobenzoyl-*N*-hydroxysuccinimide ester; BS^3, bis(sulfosuccinimidyl) suberate; EDC, 1-ethyl 3-[3-(dimethylamino)propyl]carbodiimide; sulfo-NHS, *N*-hydroxysulfosuccinimide; DTT, dithiothreitol; WT, wild type; DCIP, 2,6-dichloroindophenol.

 Published on Web 12/02/2009

E72A replacements in Pdr and Pdx, respectively, were performed using the Stratagene QuikChange kit. The mutants were purified according to procedures developed for the wild-type (WT) proteins.

Cross-Linking the Pdr−Pdx Complex. Cross-linking reagents *m*-maleimidobenzoyl-*N*-hydroxysuccinimide ester (MBS), bis(sulfosuccinimidyl) suberate (BS^3), EDC, and *N*-hydroxysulfosuccinimide (sulfo-NHS) were obtained from Thermo Scientific. Initial screening was conducted under various conditions with different protein:reagent ratios as described in the figure legends. Reaction products were separated by sodium dodecyl sulfate−polyacrylamide gel electrophoresis (SDS−PAGE) and quantified with ImageJ (*31*). Preparative quantities of the EDC-mediated conjugate between Pdr and Pdx C73S/C85S were obtained according to the following procedure. Before being mixed with Pdx, Pdr was preincubated for 1−2 h at 37 °C with a 3-fold excess of dithiothreitol (DTT) in 0.1 M sodium phosphate (pH 7.4) and 0.15 M NaCl (reaction buffer) to reduce nonspecific disulfide bonds between surface cysteines. Carboxyl groups in Pdx [4000 nmol in 2.5 mL of 0.1 M MES (pH 6.5) and 0.5 M NaCl] were activated by 10- and 25-fold molar excesses of EDC and sulfo-NHS, respectively. Sulfo-NHS improves the efficiency of the cross-linking reaction, as amine-reactive sulfo-NHS esters are less sensitive to hydrolysis. After a 15 min incubation at room temperature, the protein solution was passed through a desalting column equilibrated in the reaction buffer to remove the excess of modifying agents, immediately mixed with Pdr (Pdr:Pdx ratio of 1:10), concentrated to 0.5 mL, degassed, and kept in the dark for 4 h. The Pdr−Pdx mixture was then diluted to 10 mL with 50 mM sodium phosphate (pH 7.4) and left overnight to hydrolyze the EDC-modified groups that did not react with Pdr. The next morning, the mixture was concentrated to 1−2 mL and used for purification of the cross-linked complex.

Purification of the Cross-linked Pdr−Pdx Complex. To separate the stoichiometric Pdr−Pdx conjugate from nonlinked proteins and other byproducts of the reaction, gel filtration chromatography on HiLoad Superdex 75 (26/60) was used as the first purification step [50 mM sodium phosphate (pH 7.4) and 0.2 mM DTT, with a flow rate of 0.5 mL/min]. Fractions enriched in the 1:1 conjugate were pooled, concentrated to 1 mL, and incubated with 1 mM DTT (final concentration) for 1 h at 37 °C. The sample was then loaded on a Mono Q (5/50) FPLC ion-exchange column equilibrated in 5 mM sodium phosphate (pH 7.4) and 0.1 mM DTT with a flow rate of 0.2 mL/min. The column was first washed with 5 volumes of the loading buffer and then with 5 volumes of 40 mM phosphate (pH 7.4). The Pdr−Pdx cross-link was eluted with a linear gradient from 40 to 100 mM phosphate (pH 7.4).

Redox Activity Assays. Reductase activities of Pdr toward 2,6-dichloroindophenol (DCIP) and $K_3Fe(CN)_6$ were measured at 25 °C in 20 mM phosphate (pH 7.4) and calculated using an ε_{600} of 21 mM^{-1} cm^{-1} and an ε_{420} of 1.02 mM^{-1} cm^{-1}, respectively. Steady-state kinetics of cytochrome *c* reduction by Pdx stoichiometrically mixed (0.1 μM) or fused with Pdr (0.7 nM) was followed at 25 °C in 20 mM phosphate (pH 7.4) (ε_{550} = 21 mM^{-1} cm^{-1}).

Measurement of ET to P450cam. The first ET from reduced Pdx to P450cam was followed at ambient temperature under anaerobic conditions in carbon monoxide-saturated 20 mM phosphate (pH 7.4) containing 100 mM KCl, 0.5 mM camphor, and an oxygen scrubbing system consisting of 5 mM glucose, 1 unit/mL glucose oxidase, and 1 unit/mL catalase. Intact or cross-linked Pdr and Pdx (0.5 μM) were mixed with 2.5−30 μM P450cam in the presence of 0.3 mM NADH, and formation of the ferrous−CO adduct was monitored at 446 nm using an Applied Photophysics stopped-flow spectrophotometer.

NADH Oxidation and H_2O_2 Formation. Camphor-dependent NADH consumption was monitored at 25 °C and 340 nm (ε = 6.22 mM^{-1} cm^{-1}) in 20 mM phosphate (pH 7.5) and 0.1 M KCl. The reaction between 0.5 μM intact or conjugated Pdr and Pdx and 2.5−30 μM P450cam was initiated by 0.3 mM NADH in the absence or presence of 0.5 mM camphor. H_2O_2 formation was assessed as described elsewhere (*32*). Reactions (0.5 mL) were initiated with NADH and terminated 15 min later via addition of 1 mL of cold trichloroacetic acid (3%, w/v). H_2O_2 was determined spectrophotometrically by reaction with ferrous ammonium sulfate and KSCN.

Camphor Hydroxylation. Camphor consumption and hydroxycamphor production were analyzed using a GCT Premier time-of-flight mass spectrometer (Waters). Reactions between 2.5−15 μM P450cam and 0.5 μM intact or cross-linked Pdr and Pdx were conducted for 0−60 min at 25 °C in 20 mM phosphate (pH 7.4) containing 0.1 M KCl, 0.7 mM camphor, and 0.7 mM NADH and terminated by mixing with CH_2Cl_2, to which 0.5 mM cineole was added as an internal standard. After vortex mixing and centrifugation, the lower organic layer was transferred to a clean tube and analyzed by gas chromatography and mass spectroscopy (GC−MS) with positive chemical ionization using ammonia reagent gas. The gas chromatograph was operated with a DB-5 column (25 m) with temperature programming (50 °C at start, ramp at a rate of 10 °C/min to 290 °C). Cineole, camphor, and hydroxycamphor were identified using authentic standards and mass analysis.

Other Procedures. The extinction coefficient of the cross-linked Pdr−Pdx complex was estimated using a BCA protein assay kit (Thermo Scientific) and bovine serum albumin as a standard. Identification of the residues covalently linked by EDC was performed with the assistance of Alphalyse, Inc. In-gel protein samples were reduced and alkylated with iodoacetamide prior to digestion with trypsin, followed by MALDI-TOF peptide mass fingerprint and MALDI-TOF/TOF peptide sequencing according to standard Alphalyse procedures.

RESULTS

Screening Cross-Linking Agents. Since previous studies suggested that formation of the Pdr−Pdx complex is assisted by both ionic and nonionic interactions and steric complementarity (*13*, *19*, *20*, *23*, *24*, *27*), we tested the ability of several cross-linking reagents with different functional groups to produce Pdr−Pdx conjugates. Among the reagents tested were MBS (reacts with amino and sulfhydryl groups, 7.3 Å spacer arm), BS^3 (reacts with primary amines, 11.4 Å spacer arm), and EDC (conjugates carboxyl to amino groups, zero length). The cross-linking reactions were conducted under different conditions with various buffer compositions, pHs, ionic strengths, reagent:protein ratios, and reaction times, followed by electrophoretic separation and quantitation of the products. As seen in Figure 1, BS^3 did not produce intermolecular links but heavily modified the flavoprotein (diffused Pdr bands in lanes 6−8). MBS, on the other hand, promoted formation of a conjugate with a molecular mass of ~60 kDa. The higher than expected molecular mass (57 kDa) and significantly deformed protein bands (lanes 3−5) indicate that MBS attaches to multiple lysines

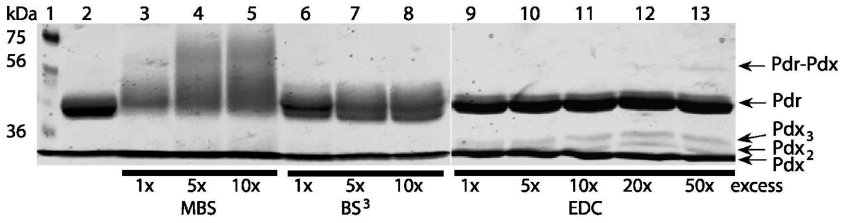

FIGURE 1: Electrophoretic analysis of the products of the MBS-, BS^3-, and EDC-mediated cross-linking reactions between Pdr and WT Pdx. Reactions were conducted at room temperature in 20 mM HEPES (pH 7.4). A 1:6 Pdr−Pdx mixture was incubated for 30 min with different amounts of the cross-linking reagents followed by product separation by SDS−PAGE: lane 1, molecular mass standards; lane 2, unmodified Pdr and Pdx.

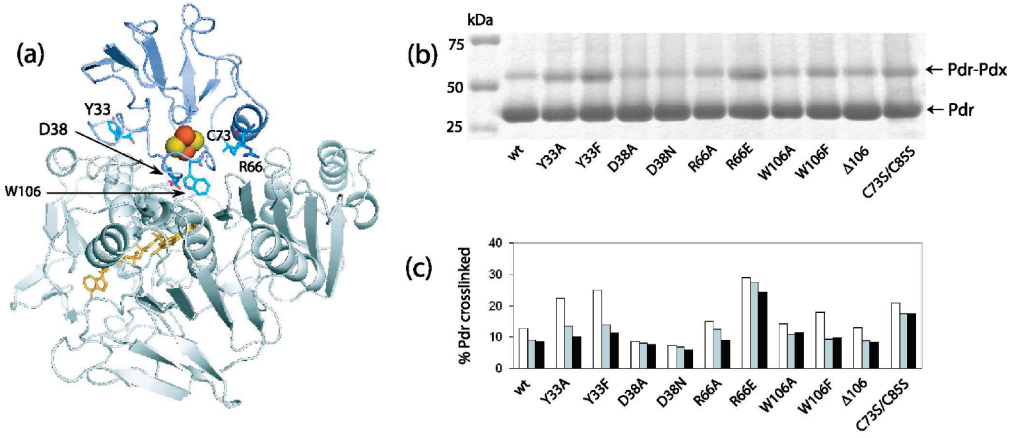

FIGURE 2: EDC-mediated cross-linking reaction between Pdr and mutants of Pdx. (a) Computer-generated model for the Pdr−Pdx ET complex (*27*) with the mutated residues displayed. Solvent inaccessible Cys85 is not shown. (b) Effect of Pdx mutations on the conjugation reaction between the oxidized partners. Pdr (60 μM) and Pdx (720 μM) were incubated for 2 h with a 200-fold excess of EDC in 20 mM HEPES (pH 7.4) under anaerobic conditions. Reaction products were separated via 10% SDS−PAGE. (c) Effect of the Pdr and Pdx redox state on the yield of the EDC-mediated cross-link, estimated as a percentage of total Pdr. Reactions between the Pdr^{ox}−Pdx^{ox} (white), Pdr^{ox}−Pdx^{red} (gray), and Pdr^{red}−Pdx^{red} (black) pairs were conducted in the absence and presence of 360 and 500 μM NADH as described above.

and cysteines on the Pdr surface. In contrast, carboxyl-reactive EDC predominantly cross-linked Pdx molecules and, most importantly, produced small amounts of a homogeneous stoichiometric Pdr−Pdx complex (~4% yield at an EDC:protein ratio of 50:1). This prompted us to focus in this study primarily on EDC.

Pdx Mutations and the Redox State of the Partners Affect the Yield of the EDC-Mediated Cross-Linking Reaction. Elevating the Pdx:Pdr and EDC:protein ratios and extending the reaction time enabled an increase in the yield of the 1:1 conjugate up to 20%. However, because of quick inactivation of WT Pdx in solution, caused by formation of intermolecular disulfide bridges and loss of the metal cluster (*28*), it was not possible to obtain sufficient amounts of the catalytically active cross-linked complex. To overcome this problem, several available mutants of Pdx were tested in an attempt to find one that could give higher conjugate yields and withstand chemical reaction and purification conditions. Among the variants investigated were D38A, D38N, Y33A, Y33F, R66A, R66E, W106A, W106F, Δ106, and C73S/C85S, whose interaction with Pdr was previously characterized (*27*, *28*). All mutated residues except Cys85 are solvent-exposed and located at the Pdr−Pdx interface in the model ET complex (Figure 2a) (*27*). As our experiments showed, deletion of the C-terminal Trp106 had virtually no effect on the EDC-mediated Pdr−Pdx cross-linking reaction; the R66A and W106A mutations had a moderate positive effect, promoting conjugation by 3−17%, whereas the Y33A, Y33F, R66E, W106F, and C73S/C85S substitutions increased the cross-link yield by 40−128%. In contrast, elimination of the negative charge on Asp38 led to a 30−42% decrease in the fusion protein formation (Figure 2b).

Given that Pdx undergoes significant redox-linked conformational reorganization, proposed to be important for the redox partner binding (*30*, *33*−*36*), we checked how reduction of the metal cluster affects the Pdr−Pdx conjugate yields. Due to fast Pdr-to-Pdx ET, it was not possible to examine the EDC-mediated reaction between the physiologically relevant pair, Pdr^{red}−Pdx^{ox}, but anaerobic addition of limited amounts of NADH sufficient only for reduction of Pdx and an excess of the reductant enabled us to monitor conjugation between the Pdr^{ox}−Pdx^{red} and Pdr^{red}−Pdx^{red} couples, respectively. These experiments revealed that, for any Pdx variant tested, the cross-link yields between the partners in the mixed or fully reduced state were lower than between the oxidized proteins (Figure 2c), with the largest redox difference observed for the Tyr33 mutants. The less pronounced difference in Pdr^{ox}−Pdx^{red} and Pdr^{red}−Pdx^{red} conjugation suggests that the redox-state change in Pdx affects the complex affinity to a greater degree than oxidation or reduction of the flavoprotein.

Although the largest amounts of the conjugate were produced with the Tyr33 and Arg66 variants, Pdx C73S/C85S was chosen for large-scale preparations because the cysteine elimination more mildly affects the electron accepting ability of Pdx (a 30% decrease vs 70% for the tyrosine and arginine substitutions) and significantly increases protein stability (*28*).

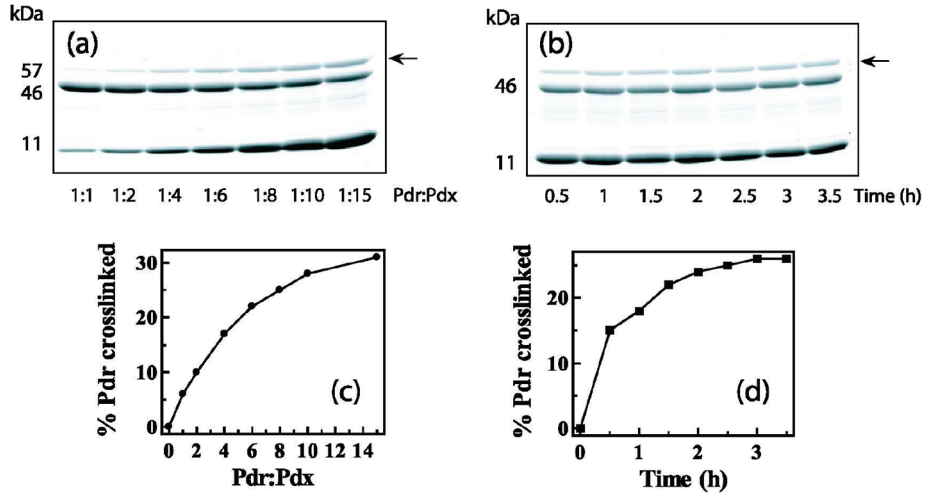

FIGURE 3: (a and b) Product separation and (c and d) yields of the EDC-mediated conjugate between Pdr and Pdx C73S/C85S. The stoichiometric Pdr−Pdx complex is denoted with arrows. Before reaction with Pdr, carboxyl groups on Pdx were activated using an EDC:sulfo-NHS:protein ratio of 100:250:1. Cross-link yields were calculated from the gel scans as a percentage of total Pdr. Reactions depicted in panel a were conducted for 3 h; the Pdr:Pdx ratio in panel b was 1:10. No conjugate formation was detected when carboxyl groups on Pdr were activated (see Figure 1S of the Supporting Information).

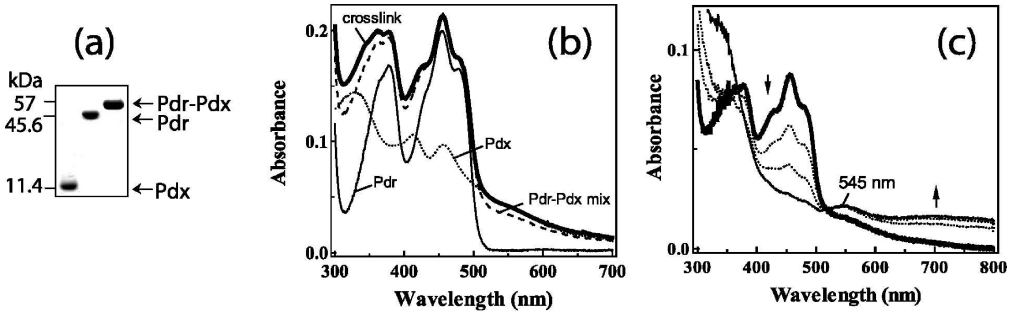

FIGURE 4: (a) SDS−PAGE gel of intact and cross-linked Pdr and Pdx C73S/C85S used for biochemical characterization. (b) Optical spectra of oxidized intact and conjugated proteins. (c) Spectral changes observed during anaerobic reduction of the cross-linked complex with a 2-fold excess of NADH. A 545 nm peak and a long-wavelength absorbance band are characteristic features of the reduced [2Fe-2S] cluster and $FADH_2$−NAD charge transfer complex, respectively.

Optimization of the Cross-Linking Reaction. To optimize the EDC-mediated reaction and prevent unnecessary exposure of the protein to chemicals, we determined what groups each partner provides during cross-linking. For this purpose, the carboxyl groups on Pdr and Pdx were alternatively activated, and after removal of an excess of the reagents, the modified and unmodified partners were mixed. These experiments showed that the Pdr−Pdx cross-link was produced only when acidic residues on Pdx were modified (Figure 3 and Figure 1S of the Supporting Information). Markedly, even at very high Pdx:Pdr ratios (up to 50:1), a stoichiometric conjugate was the major species produced (Figure 2S of the Supporting Information). This finding indicates that there may be only one preferable docking orientation between the partners. Since at Pdx:Pdr ratios of > 10:1 the yield of the desired complex increased only slightly, we ended up using a 10-fold excess of Pdx over Pdr for large-scale preparations, as described in detail in Experimental Procedures, to minimize protein waste and ease purification.

Spectral Properties of the Cross-Linked Pdr−Pdx Complex. The purified stoichiometric Pdr−Pdx C73S/C85S complex had a yellow-brown color and a spectrum resembling that of an equimolar mix of intact proteins (Figure 4a,b) with an estimated ε_{455} of 16.7 ± 0.3 mM^{-1} cm^{-1}, which is equal to a sum of the extinction coefficients for Pdr and Pdx [10.8 and 5.9 mM^{-1} cm^{-1}, respectively (*12*, *27*)]. Anaerobic reduction of the conjugate with NADH led to an absorbance decrease in the 350−500 nm range and the appearance of a 545 nm peak and a broadband in the long-wavelength region, characteristic features of the reduced [2Fe-2S] cluster and $FADH_2$−NAD charge transfer complex, respectively (Figure 4c). The flavin and iron−sulfur cofactors were quickly oxidized by air oxygen, and the resulting spectrum was identical to that taken prior addition of the reductant (not shown). On the basis of the spectral properties, we can conclude that FAD and the [2Fe-2S] cluster in the conjugated Pdr and Pdx remain redox active.

Covalently Linked Pdr and Pdx Are Competent in Electron Transfer. To evaluate how covalent linkage affects the electron transferring ability of Pdr and Pdx, we measured the NADH-dependent reduction of DCIP and $K_3Fe(CN)_6$, accepting electrons from Pdr, as well as P450cam and cytochrome *c*, receiving reducing equivalents from Pdx. Assays involving both intact and conjugated Pdr−Pdx pairs showed that cross-linked Pdr maintained more than 90% of the electron transferring ability of the intact flavoprotein (Table 1). Attachment of Pdx did not affect the K_M for NADH but increased the K_M for DCIP and $K_3Fe(CN)_6$ by factors of 3 and 5, respectively, likely due to a lesser access of the molecules to the flavoprotein active site.

The first ET from Pdx to P450cam was assayed by following formation of the ferrous−CO adduct. For the intact Pdr−Pdx mixture, the plot of k_{obs} versus P450cam concentration was

Table 1: NADH-Dependent Redox Activities of Intact and Cross-Linked Pdr

	k_{cat} (min^{-1})	$K_M^{acceptor}$ (μM)	K_M^{NADH} (μM)
	DCIP		
intact Pdr	10600 ± 600 (100%)	19 ± 3	27 ± 2
cross-linked Pdr	9700 ± 800 (92%)	60 ± 7	35 ± 3
	$K_3Fe(CN)_6$		
intact Pdr	59600 ± 5500 (100%)	63 ± 8	22 ± 3
cross-linked Pdr	54800 ± 4300 (92%)	308 ± 25	29 ± 4

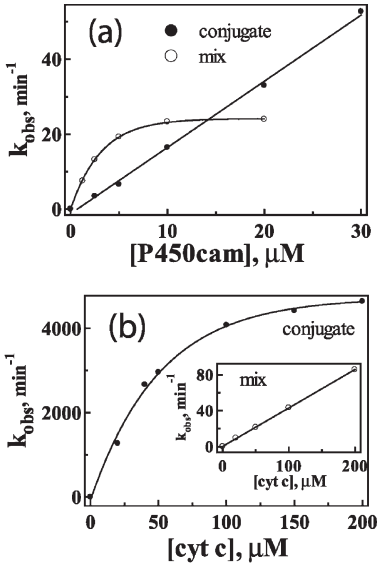

FIGURE 5: Kinetics of ET from the cross-linked and intact Pdx to P450cam (a) and cytochrome *c* (b). Reaction mixtures contained 0.5 μM fused or mixed Pdr and Pdx and various concentrations of hemoproteins. Transfer of the first electron to P450cam and formation of the ferrous−CO adduct were monitored at 446 nm by stopped-flow spectrophotometry; steady-state kinetics of cytochrome *c* reduction was followed at 550 nm. Reaction conditions are described in Experimental Procedures. Kinetic parameters calculated from the plots are listed in Table 2.

saturating, consistent with Pdx^{red} forming a complex with P450cam prior to ET. The k_{ET} and $K_d^{P450cam}$ values calculated from a hyperbolic fit were 29 min^{-1} and 2.9 μM, respectively (Figure 5a and Table 2). In sharp contrast, the cross-linked pair did not saturate within the studied P450cam concentration range, giving a second-order rate constant of 1.8×10^6 M^{-1} min^{-1}. As a basis for comparison, the linear portion of the Figure 5a plot for the reduction of P450cam by free Pdx gives an apparent bimolecular rate constant (k_{app}) of 5.3×10^6 M^{-1} min^{-1}, meaning that the cross-linked complex reduces P450cam ~3-fold more slowly. Although attached Pdr clearly perturbed formation of the Pdx−P450cam complex, its interference was compensated at saturating levels of the hemoprotein: at P450cam:Pdx ratios of ≥30:1, the Pdx-to-P450cam ET rates for the cross-linked pair approached and even exceeded those for the freely diffusible proteins.

Unlike the P450cam reduction reaction, ET to cytochrome *c* from the fused Pdr−Pdx couple was considerably more efficient than from unmodified partners (Figure 5b and Table 2). For the noncovalently linked pair, the k_{obs} versus cytochrome *c* concentration dependence was linear, with a second-order ET rate

Table 2: Kinetic Parameters for the P450cam and Cytochrome *c* Reduction Reactions Catalyzed by the Covalently Linked and Freely Diffusible Pdr−Pdx Pairs

	Pdr−Pdx cross-link	1:1 Pdr−Pdx mix
	First ET to P450cam	
k_{ET} (min^{-1})	−[a]	29 ± 2
K_d (μM)	−	2.9 ± 0.3
k (M^{-1} min^{-1})	$(1.8 \pm 0.1) \times 10^6$	−
	Cytochrome *c*	
k_{cat} (min^{-1})	5700 ± 200	−
K_M (μM)	40 ± 2	−
k (M^{-1} min^{-1})	−	$(4.3 \pm 0.3) \times 10^5$

[a]The dependence of k_{obs} on protein concentration was linear within the studied protein concentration range.

constant of 4.3×10^5 M^{-1} min^{-1}. For the fusion protein, the corresponding plot was saturating, giving k_{cat} and K_M^{cytc} values of 5700 min^{-1} and 40 μM, respectively. The k_{app} value calculated from the initial linear interval was 6.7×10^7 M^{-1} min^{-1}, indicating that the cross-linked complex reduces cytochrome *c* >150-fold faster than the intact proteins. Thus, according to the kinetic data, EDC captures the redox partner orientation optimal for the Pdr-to-Pdx and Pdx-to-cytochrome *c* but not Pdx-to-P450cam ET.

To check whether another Pdx molecule can dock and accept electrons from the cross-linked Pdr, we examined how addition of free Pdx affects P450cam and cytochrome *c* reduction. The externally added Pdx was found to proportionally increase the level of ET in the mixture of intact proteins, as expected, but had no effect on the activity of the fused complex (Figure 6). Again, this suggests that there is only one productive docking site, which is occupied by Pdx in the covalent complex, thus preventing free Pdx from properly binding to Pdr.

Cross-Linked Pdx Can Act as a Coupling Effector. The camphor hydroxylation reaction catalyzed by P450cam requires an input of two electrons. The first electron can be transferred to the hemoprotein by any reducing agent with a suitable redox potential, but only Pdx can deliver the second electron and couple ET to successful substrate turnover (*37*−*39*). To elucidate whether the cross-linked Pdx can act as an effector of the camphor hydroxylation reaction, we analyzed product formation in the reconstituted systems consisting of various amounts of P450cam and either intact or fused Pdr and Pdx. As Figure 7 demonstrates, the cross-linked Pdr−Pdx pair supports camphor hydroxylation more effectively than the intact one when high levels of P450cam are present. At P450cam:Pdx ratios of <10:1, however, ET between the unmodified partners becomes more productive (Figure 8a). Since the reaction catalyzed by P450cam can be uncoupled and lead to H_2O_2 production, we measured also the rates of camphor-dependent NADH oxidation (Figure 8b) and H_2O_2 formation. NADH consumption and camphor hydroxylation reactions supported by both intact and cross-linked Pdr and Pdx were found to be tightly coupled (92−97%), and the level of H_2O_2 production did not exceed 5%. This means that the linked Pdx not only delivers two electrons to P450cam but also efficiently operates as an effector.

Glu72^{Pdx}−Lys409^{Pdr} Is a Possible Cross-Link Site. To gain further insights into the Pdr−Pdx interaction, we attempted to identify residues linked by EDC. In-gel trypsinolysis and peptide analysis were performed in parallel for the covalently linked and intact Pdr and Pdx C73S/C85S. According to MALDI spectra (Figure 9a), a peptide with a mass of 5017 Da is detected only in the conjugate sample and could represent a link between the 1874 Da peptide of Pdx (^{67}EIGMLESVTAELKPNSR^{83}) and the 3144 Da peptide of Pdr. If this assumption is correct, Glu72 and Glu77 (underlined) are the only surface residues in Pdx that could be linked by EDC. Between these two, only Glu72 was reported to be important for the Pdr−Pdx interaction (*20*, *22*) and, according to our computer model (*27*), is in a position suitable for formation of a salt bridge with Lys409 of Pdr (Figure 9b). To test whether the Glu72^{Pdx}−Lys409^{Pdr} pair represents the EDC-cross-linked site, E72A and K409A mutations were introduced into Pdx and Pdr, respectively, and their effect on conjugation was assessed. Strikingly, elimination of the charged side chains on either Glu72 or Lys409 completely abolished formation of the cross-linked complex (Figure 9c). Unfortunately, without knowing the 3144 Da peptide sequence, we are unable to definitively conclude that the mutated residues are conjugated by EDC. Nevertheless, the inability of both E72A and K409A variants to produce even traces of the conjugates is a strong indication that Glu72 and Lys409 contribute to molecular recognition between Pdr and Pdx.

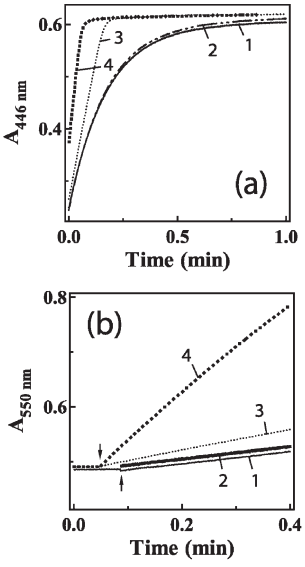

FIGURE 6: Effect of externally added Pdx on reduction of P450cam (a) and cytochrome *c* (b). In each panel, traces 1 and 2 correspond to the cross-linked Pdr and Pdx, respectively, and traces 3 and 4 to their 1:1 mixture. Traces 1 and 3 were recorded in the absence of externally added Pdx and traces 2 and 4 in the presence of 1 equiv of free Pdx. Reduction of P450cam by 0.5 μM mixed or cross-linked Pdr and Pdx was followed at 446 nm to monitor formation of the ferrous−CO adduct. For cytochrome *c* reduction, 0.1 μM mixed or 0.7 nM cross-linked Pdr and Pdx were used.

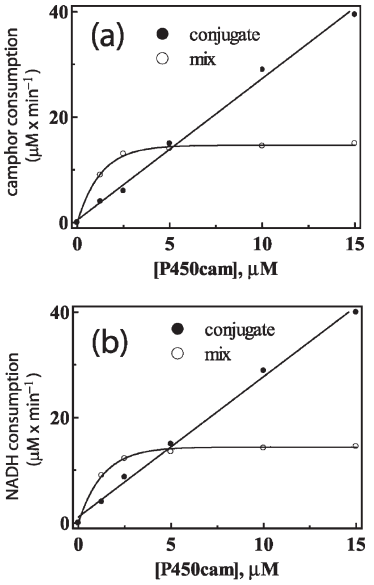

FIGURE 8: Kinetics of camphor (a) and NADH (b) consumption during turnover of 2.5−15 μM P450cam with 0.5 μM intact or conjugated Pdr and Pdx in 20 mM phosphate buffer (pH 7.4) containing 0.1 M KCl and 0.7 mM camphor. Reactions were initiated with 0.7 mM NADH and stopped 15 min later via addition of CH_2Cl_2. The organic phase was analyzed by GC−MS. The camphor concentration was determined using a calibration curve obtained with an authentic standard.

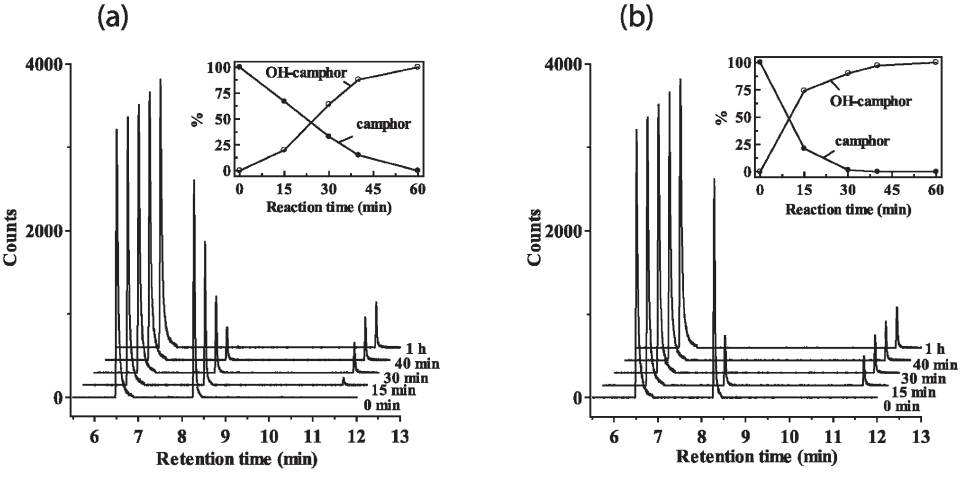

FIGURE 7: Gas−liquid chromatograms of CH_2Cl_2 extracts from the reaction mixtures containing 0.5 μM intact (a) or cross-linked Pdr and Pdx (b) and 15 μM P450cam after incubation for 0−1 h. The insets show time course of camphor consumption and hydroxycamphor formation (retention times of 8.28 and 11.46 min, respectively). The data were normalized with respect to an internal standard, cineole (retention time of 6.51 min).

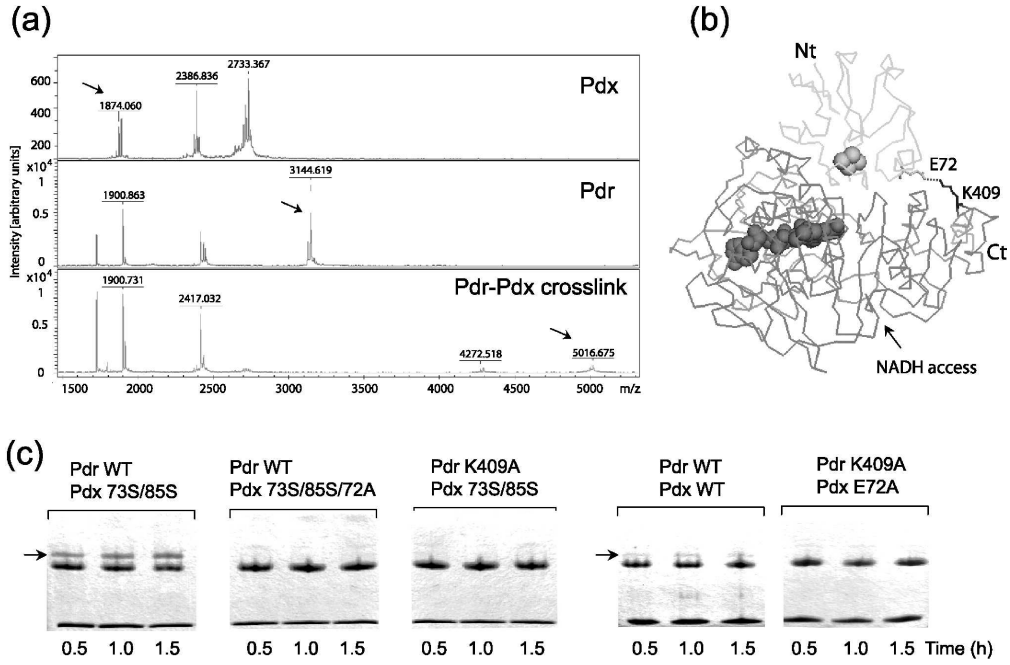

FIGURE 9: (a) MALDI spectra of tryptic digests of intact and cross-linked Pdr and Pdx (linear mode). A peptide with a mass of 5017 Da is detected only in the conjugate sample and could represent a link between the 1874 Da peptide of Pdx (^{67}EIGMLESVTAELKPNSR^{83}) and the 3144 Da peptide of Pdr (shown by arrows). Glu72 and Glu77 from the 1874 Da peptide (underlined) are the only surface accessible acidic residues in Pdx that could be linked by EDC. (b) Computer-generated model for the Pdr−Pdx ET complex (*27*), according to which the Glu72^{Pdx}−Lys409^{Pdr} pair (in stick representation) is positioned close enough to form a water-mediated salt bridge. In this molecular orientation, the entrance to the NADH access channel (denoted with an arrow) is opposite to the Pdx docking site. Positions of the C- and N-termini of Pdr and Pdx, respectively, are shown to demonstrate that the length of the linker in the Pdr−(TDGASSS)−Pdx fusion protein genetically engineered by Sibbesen et al. (*51*) is insufficient to allow the partners to dock in the depicted conformation, likely captured by EDC. (c) K409A and E72A mutations completely abolish formation of the EDC-mediated cross-link (denoted with arrows). Aliquots were taken from the reaction mixtures with a Pdr:Pdx ratio of 10:1 at different times and separated by 5−15% SDS−PAGE.

DISCUSSION

Cross-linking reagents are widely used for studying protein−protein interactions and have found success in trapping various ET partners (*40*−*45*). Interprotein ET takes place upon formation of short-lived electron donor−acceptor complexes, which can be captured together by highly reactive functional groups of the cross-linkers. In this study, we utilized a cross-linking approach to gain further insight into the mechanism of molecular recognition and interprotein ET in the Pdr−Pdx pair. Different reagents were tested for their ability to produce a functionally active 1:1 complex, among which EDC was found to be the most effective. This was not surprising because this chemical was successfully used to covalently link several other ferredoxin−ferredoxin reductase pairs (*43*, *46*−*49*). In our study, experiments with EDC were conducted under conditions close to optimal for the Pdr-to-Pdx ET [~0.3 μM ionic strength (*24*)] and led to several important observations.

First, the yields of the EDC-mediated cross-linked complex allowed us to probe the importance of various residues and protein redox state on the Pdr−Pdx association and relate these observations to kinetic results (*27*). This analysis showed that all Pdx mutations except Δ106 lower the FAD-to-[2Fe-2S] ET rate and enhance the binding affinity of the iron−sulfur protein, with the mutational effects decreasing in the following order: R66E > R66A > Y33F > Y33A > D38N > D38A > W106A > W106F. In agreement with the kinetic data, deletion or substitution of Trp106 was found to have a small or no influence on formation of the the cross-link, supporting the notion that the C-terminal tryptophan is not critical for Pdr−Pdx association. In contrast to the kinetic data, predicting a higher binding affinity for the Asp38 mutants, we saw a significant decrease in the level of fusion protein production when the negative charge at position 38 was eliminated. A more pronounced effect of the isosteric D38N replacement over D38A was observed in both studies, implying that the negative charge rather than the length of the side chain at residue 38 is critical for the Pdr−Pdx association. According to the computer model, the Asp38 carboxyl group is hydrogen bonded to the amide nitrogen of Ala51^{Pdr}, although formation of a salt bridge between the aspartate and nearby Arg65, Lys339, or Arg310 of Pdr is also possible (*27*). Contrary to the Asp38 mutations, the R66E replacement caused a >2-fold increase in the conjugate yield, which may be the result of both misorientation and formation of a novel salt bridge that could be linked by EDC. The pronounced effects of the charge removal or reversal on Asp38 and Arg66 emphasize the importance of electrostatic forces in the Pdr−Pdx association that, when perturbed, appear to misorient the partners and change the complex geometry, disfavoring ET (*27*). The Tyr33 replacements, on the other hand, not only strongly promoted the cross-linking reaction but also increased its redox sensitivity. In accord with the crystallographic data (*30*), this suggests that the Tyr33 region of Pdx undergoes redox-linked conformational rearrangement that may change the binding affinity of Pdx. That redox-linked changes in Pdx affect Pdr−Pdx association follows also from comparison of the Pdr^{ox}−Pdx^{ox}, Pdr^{ox}−Pdx^{red}, and Pdr^{red}−Pdx^{red} conjugate yields, showing that Pdx^{red} has the lowest affinity for Pdr in a manner independent of the redox state of the flavoprotein. This property of Pdx may be physiologically important, as it would decrease the lifetime of transient complexes with Pdr, thus freeing Pdx^{red} to bind and reduce P450cam, completing the redox cycle.

Second, having determined that carboxyl groups of Pdx interact with basic residues of Pdr, we went one step further and identified $Glu72^{Pdx}$ and $Lys409^{Pdr}$ as a possible EDC linkage site. While formation of multiple conjugation sites is possible [there is an additional unique peak with a mass of 4272 Da in the MALDI spectrum of the cross-linked species (Figure 9a)], our conclusion agrees well not only with the chemical modification and mutagenesis studies, showing that the 55−83 peptide in Pdx is the major EDC modification site (*13*) and Glu72 is critical for the Pdr−Pdx association (*20*, *22*), but also with the computer modeling results predicting formation of a $Glu72^{Pdx}$−$Lys409^{Pdr}$ salt bridge (*27*). Being peripherally located and ~12 Å in length, the glutamate−lysine link could provide Pdx some motional freedom that may be required for proper ET to the electron acceptors.

Third, utilization of EDC and Pdx C73S/C85S, the most stable mutant competent in ET, enabled us to obtain a fusion protein in amounts sufficient for biochemical characterization. Analysis of the catalytic properties of the purified complex revealed that the attached flavo- and iron−sulfur proteins remain functionally active. Moreover, when linked, Pdx reduced cytochrome *c* 150-fold faster than the intact protein. This drastic difference suggests that, in the overall reaction, the Pdr-to-Pdx ET is the rate-limiting step. In the fusion protein, this step becomes intramolecular and greatly enhanced due to the proximity of the redox centers. The high ET rates mean also that the cytochrome *c*-binding site in the linked Pdx remains accessible or/and the iron−sulfur protein has some degree of motional freedom and can reorient during turnover to optimize interaction with both partners. In contrast, ET from the linked Pdx to P450cam was partially impaired and became more efficient than that from the intact iron−sulfur protein only in the presence of a large excess of P450cam. Together with the lack of a stimulating effect of externally added Pdx on the cytochrome *c* and P450cam reduction catalyzed by the fusion protein, this suggests that (i) the P450cam binding step rather than ET from the linked Pdx to the heme iron is perturbed, (ii) there is only one Pdx docking site leading to a successful FAD-to-[2Fe-2S] ET, and (iii) the productive Pdr−Pdx orientation is favorable for cytochrome *c* but not P450cam reduction. The impairment of interaction with P450cam could be due to spatial overlap of the Pdr- and P450cam-binding sites on Pdx (*23*) and the limited ability of the cross-linked Pdx to reorient toward the larger electron acceptor. The latter suggestion supports the shuttle mechanism, according to which Pdx must form transient complexes and dissociate from both partners to efficiently shuttle electrons.

Finally, our study demonstrates that Pdx in the covalent complex can still serve its effector role by fully supporting camphor hydroxylation with no uncoulpling of ET from hydroxylation. It is generally thought that the effector role of Pdx is due to proper docking of Pdx to P450cam via the C-terminal Trp106 (*37*−*39*), which may result in specific structural changes in the hemoprotein required for catalysis (*50*). Therefore, Pdx in the covalent complex must be able to induce the same types of functionally important structural changes as free Pdx. If, as the prevalent view holds, the same or overlapping surface patches of Pdx interact with both Pdr and P450cam, then in the covalent complex Pdx must be able to reorient to properly dock to P450cam. This is feasible on the basis of our Pdr−Pdx model and the cross-linking results since (i) the cross-linking site appears to be at the very edge of the complex which could allow considerable freedom of motion and (ii) Trp106 has no effect on the Pdr−Pdx interaction and, therefore, is unlikely to be trapped at their interface and could be available for P450cam binding. The kinetic behavior of both P450cam reduction and camphor hydroxylation by the covalent complex, neither of which is saturated at high P450cam concentrations, could be explained by such a model. Pdx in the covalent complex spends a very small fraction of time in an orientation favorable for ET to P450cam, thus considerably lowering the effective concentration of Pdx for ET to P450cam. As a result, substantially higher concentrations of the Pdr−Pdx conjugate are required to achieve high rates of P450cam reduction and camphor hydroxylation.

Interestingly, at saturating levels of P450cam, the catalytic turnover of the EDC-linked Pdr−Pdx complex is almost 1 order of magnitude higher than that of the Pdr−(TDGASSS)−Pdx fusion protein genetically engineered by Sibbesen et al. (*51*) (1.8×10^6 and 1.7×10^5 min^{-1}, respectively). On the basis of our computer model (Figure 9b), the large difference in the activity can be explained by misorientation of Pdx in the latter complex, as the length of the seven-residue linker between the C-terminus of Pdr and the N-terminus of Pdx is too short to allow the partners to dock in the productive conformation captured by EDC. The suboptimal Pdr−Pdx geometry may lead to a less efficient Pdr-to-Pdx ET and, as a consequence, decrease P450cam turnover.

It should be emphasized also that the NADH access channel in the Pdr−Pdx pair linked through the $Lys409^{Pdr}$−$Glu72^{Pdx}$ pair would be opposite to the Pdx docking site (Figure 9b). In this molecular orientation, binding of the pyridine nucleotide would not interfere with Pdx association and/or dissociation, and thus, ternary NAD(H)−$Pdr^{ox/red}$−$Pdx^{ox/red}$ complexes could be formed. The latter possibility and the proximity of the flavin and metal cofactors, ensuring fast electron exchange, allow us to hypothesize that some reactions catalyzed by the Pdr−Pdx fusion protein may proceed via a compulsory-order mechanism, suggested by Reipa et al. for the intact pair (*52*). According to this mechanism, the ET pathway includes series of steps that must occur in a specified order: the two-electron reduction of Pdr with NADH takes place first, followed by two consecutive $Pdr^{red} \rightarrow Pdx^{ox}$ and $Pdr^{sq} \rightarrow Pdx^{ox}$ one-electron transfers (see Figure 9 in ref *52*). Since Pdr does not stabilize the FAD semiquinone (*53*), transient formation of Pdr^{sq} is the major assumption of the proposed mechanism. Thus far, formation of a short-lived blue, neutral FAD semiquinone in Pdr was detected only during laser flash-induced reduction with 5-deazariboflavin, which was followed by disproportionation of the one-electron-reduced species into the two-electron-reduced and oxidized forms with the rate constant ranging from 50 to 250 s^{-1}, depending on the reaction conditions (*24*). Considering fast ET from the cross-linked Pdx to cytochrome *c* (k_{cat} = 63 s^{-1}), it is plausible to conclude that Pdr^{sq}−Pdx^{red} and Pdr^{ox}−Pdx^{red} pairs are catalytically competent intermediates involved in cytochrome *c* reduction (Figure 10). During camphor hydroxylation, however, the rate-limiting Pdx-to-P450cam ET step proceeds considerably slower that the FAD semiquinone disproportionation, which may result in conversion of the Pdr^{sq}−Pdx^{red} species to Pdr^{ox}−Pdx^{red} and Pdr^{red}−Pdx^{red} before the P450cam reduction takes place. In this case, the $Pdr^{red}_{(NAD)}$−Pdx^{red} and Pdr^{ox}−Pdx^{red} species would be the major intermediates delivering electrons to P450cam, and the reaction would obey the branched rather than compulsory-order mechanism. Precise identification of the ET pathways and intermediates formed during redox cycling of the covalent Pdr−Pdx complex requires further investigations and may be a

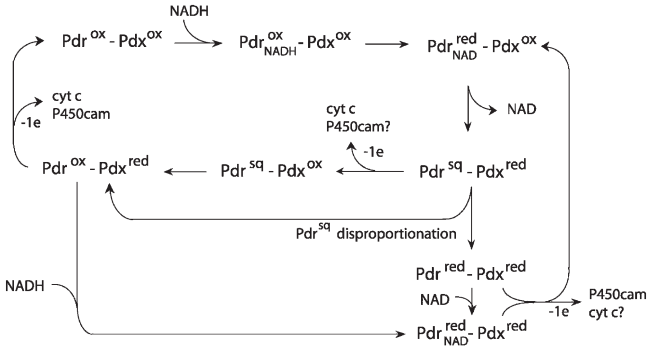

FIGURE 10: Possible ET pathways and intermediates formed during redox cycling of the covalent Pdr−Pdx complex. For simplicity, the NAD-bound Pdr^{sq}−Pdx^{red}, Pdr^{sq}−Pdx^{ox}, Pdr^{ox}−Pdx^{red}, and Pdr^{ox}−Pdx^{ox} species are not included in the scheme. On the basis of the kinetic results obtained in this study and the rate of FAD semiquinone disproportionation estimated previously (*24*), the Pdr^{sq}−Pdx^{red} and Pdr^{ox}−Pdx^{red} species are proposed to be the major forms reducing cytochrome *c*, wherein the $Pdr^{red}{}_{(NAD)}$−Pdx^{red} and Pdr^{ox}−Pdx^{red} forms are the likely intermediates donating electrons to P450cam.

challenging task due to significant spectral overlap among the flavin, iron−sulfur, and heme groups.

Summarizing our results, we conclude that the EDC-captured complex is physiologically relevant and represents a suitable model for mechanistic and structural studies, and that high specificity of the Pdr−Pdx redox couple is defined by finely tuned interactions at the protein−protein interface and the existence of only one docking orientation leading to successful ET.

ACKNOWLEDGMENT

We thank Dr. John Greaves for assistance with GC−MS.

SUPPORTING INFORMATION AVAILABLE

SDS−PAGE separation of the products of the EDC-mediated conjugation reaction between Pdx and activated Pdr conducted at various protein:protein ratios and reaction times (Figure 1S) and products of the EDC cross-linking reaction between Pdr and activated Pdx conducted at a Pdr:Pdx ratio of 1:50 (Figure 2S). This material is available free of charge via the Internet at http://pubs.acs.org.

REFERENCES

1. Senda, T., Yamada, T., Sakurai, N., Kubota, M., Nashizaki, T., Masai, T., Fukuda, M., and Mitsui, Y. (2000) Crystal structure of NADH-dependent ferredoxin reductase component in biphenyl dioxygenase. *J. Mol. Biol. 304*, 397–410.
2. Katagiri, M., Ganguli, B. N., and Gunsalus, I. C. (1968) A soluble cytochrome P450 functional in methylene hydroxylation. *J. Biol. Chem. 243*, 3543–3546.
3. Kadkhodayan, S., Coulter, E. D., Maryniak, D. M., Bryson, T. A., and Dawson, J. H. (1995) Uncoupling oxygen transfer and electron transfer in the oxygenation of camphor analogues by cytochrome P450cam. Direct observation of an intermolecular isotope effect for substrate C-H activation. *J. Biol. Chem. 270*, 28042–28048.
4. Reipa, V., Mayhew, M. P., and Vilker, V. L. (1997) A direct electrode-driven P450 cycle for biocatalysis. *Proc. Natl. Acad. Sci. U.S.A. 94*, 13554–13558.
5. Mayhew, M. P., Reipa, V., Holden, M. J., and Vilker, V. L. (2000) Improving the cytochrome P450 enzyme system for electrode-driven biocatalysis of styrene epoxidation. *Biotechnol. Prog. 16*, 610–616.
6. Yan, D. Z., Liu, H., and Zhou, N. Y. (2006) Conversion of *Sphingobium chlorophenolicum* ATCC 39723 to a hexachlorobenzene degrader by metabolic engineering. *Appl. Environ. Microbiol. 72*, 2283–2286.
7. Iwakiri, R., Yoshihira, K., Ngadiman, Futagami, T., Goto, M., and Furukawa, K. (2004) Total degradation of pentachloroethane by an engineered *Alcaligenes* strain expressing a modified camphor monooxygenase and a hybrid dioxygenase. *Biosci., Biotechnol., Biochem. 68*, 1353–1356.
8. Bell, S. G., Chen, X., Xu, F., Rao, Z., and Wong, L. L. (2003) Engineering substrate recognition in catalysis by cytochrome P450cam. *Biochem. Soc. Trans. 31*, 558–562.
9. Jones, J. P., O'Hare, E. J., and Wong, L. L. (2001) Oxidation of polychlorinated benzenes by genetically engineered CYP101 (cytochrome P450cam). *Eur. J. Biochem. 268*, 1460–1467.
10. Wackett, L. P. (1995) Recruitment of co-metabolic enzymes for environmental detoxification of organohalides. *Environ. Health Perspect. 103*, 45–48.
11. Manchester, J. I., and Ornstein, R. L. (1995) Enzyme-catalyzed dehalogenation of pentachloroethane: Why F87W-cytochrome P450cam is faster than wild type. *Protein Eng. 8*, 801–807.
12. Sevrioukova, I. F., and Poulos, T. L. (2002) Putidaredoxin reductase: A new function for an old protein. *J. Biol. Chem. 277*, 25831–25839.
13. Geren, L., Tuls, J., O'Brien, P., Millett, F., and Peterson, J. A. (1986) The involvement of carboxylate groups of putidaredoxin in the reaction with putidaredoxin reductase. *J. Biol. Chem. 261*, 15491–15495.
14. Bernhardt, R., and Gunsalus, I. C. (1992) Reconstitution of cytochrome P4502B4 (LM2) activity with camphor and linalool monooxygenase electron donors. *Biochem. Biophys. Res. Commun. 187*, 310–317.
15. Bell, S. G., and Wong, L. L. (2007) P450 enzymes from the bacterium *Novosphingobium aromaticivorans*. *Biochem. Biophys. Res. Commun. 360*, 666–672.
16. Chun, Y. J., Shimada, T., Waterman, M. R., and Guengerich, F. P. (2006) Understanding electron transport systems of *Streptomyces* cytochrome P450. *Biochem. Soc. Trans. 34*, 1183–1185.
17. Roome, P. W., and Peterson, J. A. (1988) The oxidation of reduced putidaredoxin reductase by oxidized putidaredoxin. *Arch. Biochem. Biophys. 266*, 41–50.
18. Gerber, N. C., and Sligar, S. G. (1994) A role for Asp251 in cytochrome P450cam oxygen activation. *J. Biol. Chem. 269*, 4260–4266.
19. Aoki, M., Ishimori, K., Fukada, H., Takahashi, K., and Morishima, I. (1998) Isothermal titration calorimetric studies on the associations of putidaredoxin to NADH-putidaredoxin reductase and P450cam. *Biochim. Biophys. Acta 1384*, 180–188.
20. Aoki, M., Ishimori, K., and Morishima, I. (1998) Roles of negatively charged surface residues of putidaredoxin in interactions with redox partners in P450cam monooxygenase system. *Biochim. Biophys. Acta 1386*, 157–167.
21. Aoki, M., Ishimori, K., and Morishima, I. (1998) NMR studies of putidaredoxin: Associations of putidaredoxin with NADH-putidaredoxin reductase and cytochrome P450cam. *Biochim. Biophys. Acta 1386*, 168–178.
22. Aoki, M., Ishimori, K., Morishima, I., and Wada, Y. (1998) Roles of valine-98 and glutamic acid-72 of putidaredoxin in the electron-transfer complexes with NADH-putidaredoxin reductase and P450cam. *Inorg. Chim. Acta 272*, 80–88.
23. Holden, M., Mayhew, M., Bunk, D., Roitberg, A., and Vilker, V. (1997) Probing the interactions of putidaredoxin with redox partners in camphor P450 5-monooxygenase by mutagenesis of surface residues. *J. Biol. Chem. 272*, 21720–21725.
24. Sevrioukova, I. F., Hazzard, J. T., Tollin, G., and Poulos, T. L. (2001) Laser flash induced electron transfer in P450cam monooxygenase: Putidaredoxin reductase−putidaredoxin interaction. *Biochemistry 40*, 10592–10600.
25. Purdy, M. M., Koo, L. S., Ortiz de Montellano, P. R., and Klinman, J. P. (2004) Steady-state kinetic investigation of cytochrome P450cam: Interaction with redox partners and reaction with molecular oxygen. *Biochemistry 43*, 271–281.
26. Ivanov, Y. D., Kanaeva, I. P., Karuzina, I. I., Archakov, A. I., Hoa, G. H., and Sligar, S. G. (2001) Molecular recognition in the P450cam monooxygenase system: Direct monitoring of protein-protein interactions by using optical biosensor. *Arch. Biochem. Biophys. 391*, 255–264.
27. Kuznetsov, V. Y., Blair, E., Farmer, P. J., Poulos, T. L., Pifferitti, A., and Sevrioukova, I. F. (2005) The putidaredoxin reductase-putidaredoxin electron transfer complex: Theoretical and experimental studies. *J. Biol. Chem. 280*, 16135–16142.

28. Sevrioukova, I. F., Garcia, C., Li, H., Bhaskar, B., and Poulos, T. L. (2003) Crystal structure of putidaredoxin, the [2Fe-2S] component of the P450cam monooxygenase system from *Pseudomonas putida*. *J. Mol. Biol. 333*, 377–392.
29. Sevrioukova, I. F., Li, H., and Poulos, T. L. (2004) Crystal structure of putidaredoxin reductase from *Pseudomonas putida*, the final structural component of the cytochrome P450cam monooxygenase. *J. Mol. Biol. 336*, 889–902.
30. Sevrioukova, I. F. (2005) Redox-dependent structural reorganization in putidaredoxin, a vertebrate-type [2Fe-2S] ferredoxin from *Pseudomonas putida*. *J. Mol. Biol. 347*, 607–621.
31. Abramoff, M. D., Magelhaes, P. J., and Ram, S. J. (2004) Image processing with ImageJ. *Biophotonics Int. 11*, 36–42.
32. Hildebrandt, A. G., Roots, I., Tjoe, M., and Heinemeyer, G. (1978) Hydrogen peroxide in hepatic microsomes. *Methods Enzymol. 52*, 342–350.
33. Jain, N. U., and Pochapsky, T. C. (1998) Redox dependence of hyperfine-shifted ^{13}C and ^{15}N resonances in putidaredoxin. *J. Am. Chem. Soc. 120*, 12984–12985.
34. Sari, N., Holden, M. J., Mayhew, M. P., Vilker, V. L., and Coxon, B. (1999) Comparison of backbone dynamics of oxidized and reduced putidaredoxin by ^{15}N NMR relaxation measurements. *Biochemistry 38*, 9862–9871.
35. Pochapsky, T. C., Kostic, M., Jain, N., and Pejchal, R. (2001) Redox-dependent conformational selection in a $Cys_4Fe_2S_2$ ferredoxin. *Biochemistry 40*, 5602–5614.
36. Jain, N. U., Tjioe, E., Savidor, A., and Boulie, J. (2005) Redox-dependent structural differences in putidaredoxin derived from homologous structure refinement via residual dipolar couplings. *Biochemistry 44*, 9067–9078.
37. Tyson, C. A., Lipscomb, J. D., and Gunsalus, I. C. (1972) The role of putidaredoxin and P450cam in methylene hydroxylation. *J. Biol. Chem. 247*, 5777–5784.
38. Sligar, S. G., Debrunner, P. G., Lipscomb, J. D., Namtvedt, M. J., and Gunsalus, I. C. (1974) A role of the putidaredoxin COOH-terminus in P450cam (cytochrome m) hydroxylations. *Proc. Natl. Acad. Sci. U.S. A. 71*, 3906–3910.
39. Lipscomb, J. D., Sligar, S. G., Namtvedt, M. J., and Gunsalus, I. C. (1976) Autooxidation and hydroxylation reactions of oxygenated cytochrome P450cam. *J. Biol. Chem. 251*, 1116–1124.
40. Mauk, M. R., and Mauk, A. G. (1989) Crosslinking of cytochrome *c* and cytochrome b_5 with a water-soluble carbodiimide. Reaction conditions, product analysis and critique of the technique. *Eur. J. Biochem. 186*, 473–486.
41. Kumar, M. A., and Davidson, V. L. (1990) Chemical cross-linking study of complex formation between methylamine dehydrogenase and amicyanin from *Paracoccus denitrificans*. *Biochemistry 29*, 5299–52304.
42. Qin, L., and Kostic, N. M. (1993) Importance of protein rearrangement in the electron-transfer reaction between the physiological partners cytochrome *f* and plastocyanin. *Biochemistry 32*, 6073–6080.
43. Pirola, M. C., Monti, F., Aliverti, A., and Zanetti, G. (1994) A functional heterologous electron-transfer protein complex: *Desulfovibrio vulgaris* flavodoxin covalently linked to spinach ferredoxin-$NADP^+$ reductase. *Arch. Biochem. Biophys. 311*, 480–486.
44. Lelong, C., Boekema, E. J., Kruip, J., Bottin, H., Rogner, M., and Setif, P. (1996) Characterization of a redox active cross-linked complex between cyanobacterial photosystem I and soluble ferredoxin. *EMBO J. 15*, 2160–2168.
45. Correia, C., Monzani, E., Moura, I., Lampreia, J., and Moura, J. J. (1999) Cross-linking between cytochrome c_3 and flavodoxin from *Desulfovibrio gigas*. *Biochem. Biophys. Res. Commun. 256*, 367–371.
46. Lambeth, J. D., Geren, L. M., and Millett, F. (1984) Adrenodoxin interaction with adrenodoxin reductase and cytochrome P450scc. Cross-linking of protein complexes and effects of adrenodoxin modification by 1-ethyl-3-(3-dimethylaminopropyl)carbodiimide. *J. Biol. Chem. 259*, 10025–10029.
47. Privalle, L. S., Privalle, C. T., Leonardy, N. J., and Kamin, H. (1985) Interactions between spinach ferredoxin-nitrite reductase and its substrates. Evidence for the specificity of ferredoxin. *J. Biol. Chem. 260*, 14344–14350.
48. Vieira, B. J., Colvert, K. K., and Davis, D. J. (1986) Chemical modification and cross-linking as probes of regions on ferredoxin involved in its interaction with ferredoxin:NADP reductase. *Biochim. Biophys. Acta 851*, 109–122.
49. Muller, E. C., Lapko, A., Otto, A., Muller, J. J., Ruckpaul, K., and Heinemann, U. (2001) Covalently crosslinked complexes of bovine adrenodoxin with adrenodoxin reductase and cytochrome P450scc. Mass spectrometry and Edman degradation of complexes of the steroidogenic hydroxylase system. *Eur. J. Biochem. 268*, 1837–1843.
50. Pochapsky, S. S., Pochapsky, T. C., and Wei, J. W. (2003) A model for effector activity in a highly specific biological electron transfer complex: The cytochrome P450cam-putidaredoxin couple. *Biochemistry 42*, 5649–5656.
51. Sibbesen, O., De Voss, J. J., and Montellano, P. R. O. (1996) Putidaredoxin reductase-putidaredoxin-cytochrome P450cam triple fusion protein. Construction of a self-sufficient *Escherichia coli* catalytic system. *J. Biol. Chem. 271*, 22462–22469.
52. Reipa, V., Holden, M. J., and Vilker, V. L. (2007) Association and redox properties of the putidaredoxin reductase-nicotinamide adenine dinucleotide complex. *Biochemistry 46*, 13235–13244.
53. Roome, P. W., and Peterson, J. A. (1988) The reduction of putidaredoxin reductase by reduced pyridine nucleotides. *Arch. Biochem. Biophys. 266*, 32–40.